Water mobility during drying of hard and soft type latex

Progress in Organic Coatings 123 (2018) 111–119

Contents lists available at ScienceDirect

Progress in Organic Coatings

journal homepage: www.elsevier.com/locate/porgcoat

Water mobility during drying of hard and soft type latex: Systematic GARField ^{1}H NMR relaxometry studies

Benjamin Voogt[a], Henk Huinink[a,*], Bart Erich[a,b], Jurgen Scheerder[c], Paul Venema[d], Olaf Adan[a,b]

[a] Department of Applied Physics, Eindhoven University of Technology, P.O. Box 513, Eindhoven, The Netherlands
[b] TNO (The Netherlands Organization for Applied Scientific Research), P.O. Box 49, Delft, The Netherlands
[c] DSM Coating Resins, P.O. Box 123, Waalwijk, The Netherlands
[d] Laboratory of Physics and Physical Chemistry of Foods, Wageningen University, Wageningen, The Netherlands

ARTICLE INFO

Keywords:
Latex drying
T_g
GARField ^{1}H NMR
Relaxometry
Water mobility

ABSTRACT

GARField ^{1}H NMR relaxometry experiments were done to study the drying process of two latices with different polymer T_g and to elucidate water mobility behavior during this process. It was found that the hard type latex, with a polymer T_g above room temperature, dries faster than the soft type latex, with a polymer T_g below room temperature. Diffusion measurements by means of echo time variations at different moments in the drying process show that water auto-diffusion decreases with increasing solid content of the latex independent of particle T_g. Two pools of protons with different mobilities were observed based on transversal relaxation T_2. Determination of the long $T_{2,long}$'s and short $T_{2,short}$'s of both latex dispersions and their respective proton densities during drying at 80% *RH* showed evidence of particle deformation for the soft type latex and the absence thereof for the hard type latex. Additional drying of the resulting coatings with anhydrous $CaCl_2$ showed a higher porosity for the hard type coating based on the proton distribution profile width. Moreover, two domains with different polymer proton mobilities are found for both coatings that are both plasticized by water at 80% *RH*. This is more apparent for the hard type coating, suggesting that a more hydrophilic polymer gives a higher degree of plasticization.

1. Introduction

Paints are probably the most abundantly used form of coating materials in the world. Apart from the aesthetic value, it can provide substrates with the necessary protection against external influences. Examples are the prevention of wood rot and metal corrosion due to the continued exposure to weather phenomena, such as rain, wind, and UV-light.

In the past decades, innovations in paint technology have been focused on the switch from solventborne to waterborne coatings, mainly driven by regulatory laws. Over the years, this development has led to the complete elimination on the use of organic solvents for paints. The development of latex was mainly enabling this switch to waterborne paints [1].

Latex is an aqueous dispersion of polymer particles, generally submicrometer sized, that upon drying form a network and give the coating its mechanical, chemical and physical properties. This film formation process takes place in a sequence of stages. First, particles are concentrated through the evaporation of water and colloidal stability by repulsion is overcome [2]. Next, particle deformation occurs decreasing the void volume between the particles [3]. Finally, the formation of a coherent coating is driven by the interdiffusion of individual polymer chains.

Studies on polymer interdiffusion are rather limited and are mostly done by the use of the fluorescence resonance energy transfer technique (FRET), often applied by Winnik and co-workers. With this, many factors that can influence the interdiffusion process, such as polymer T_g, are investigated [4–6].

The polymer T_g is directly related to its mobility. To study this, only a few techniques are available. The aforementioned FRET technique gives information on the polymer interdiffusion, but lacks the possibility to study polymer mobility changes during a drying process. Another technique used is the quartz crystal microbalance (QCM) to probe viscoelastic properties of cross-linking alkyd resins [7]. This technique could be used to study T_g and polymer mobility decrease. A major limitation of QCM, however, is the limited thickness of the applied coating ($< 2\,\mu m$).

GARField ^{1}H NMR can be used to study coatings up to 400 µm thickness and has been used previously to study the drying behavior of latices [8,9]. In a recent study, it was used to investigate the drying

* Corresponding author.
E-mail address: h.p.huinink@tue.nl (H. Huinink).

https://doi.org/10.1016/j.porgcoat.2018.06.011
Received 9 March 2018; Received in revised form 16 May 2018; Accepted 15 June 2018

Table 1
Monomer compositions (wt.%) of the latices used for this study.

Latex	Butylacrylate	Methyl methacrylate	Methacrylic acid
Hard type	25	70	5
Soft type	54.5	40.5	5

Table 2
Physical characteristics of the latices. Z_{av} is the average particle diameter, Đ the polydispersity index of the size distribution and T_g the glass transition temperature of the latex.

Latex	Z_{av} (nm)	Đ	T_g (°C)	Solids fraction (wt%)
Hard type	47.3	0.118	75.3	37.0
Soft type	57.0	0.253	18.6	37.0

behavior of latices with various particle T_g's, showing the effect of skin formation on the drying rate of latex [10]. It is an ideal technique to study water distributions and the drying rate of thin wet films. In addition, using an Ostroff–Waugh pulse sequence, information is provided on the transversal relaxation (T_2 relaxation) of water and polymer, which is directly linked to the mobility of both phases. Erich et al. [11] successfully used GARField ^{1}H NMR to show the decrease in T_2 relaxation of alkyd resins due to cross-linking of the fatty acids. For latex, where film formation occurs due to interdiffusion of polymers rather than cross-linking, such mobility studies have not been done before.

Although water distributions in drying latex dispersions have been studied extensively before with GARField ^{1}H NMR [7,8,10,12,13] no systematic study has been done before on the mobility of water in such systems. In the present study the drying behavior of two acrylic latices with T_g's lower (soft type) and higher (hard type) than room

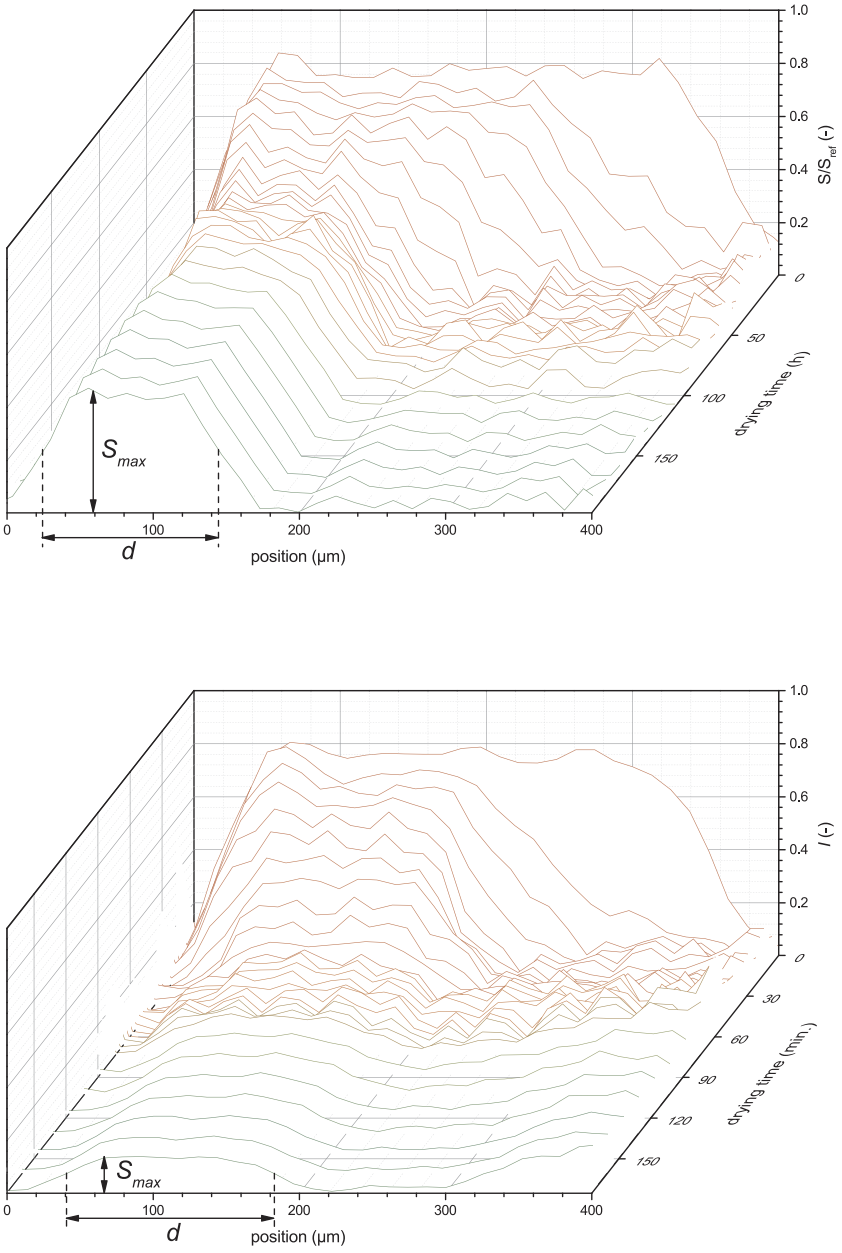

Fig. 1. Proton distribution profiles of soft type (top) and hard type (bottom) latex. The profiles at t_{drying} = 0 was obtained using an average of 256 measurements. During drying at 80% *RH*, the first 20 drying profiles and the subsequent 10 drying profiles were obtained using averages of 64 and 256 measurements respectively. To reduce noise further, a moving average of 4 drying profiles was used. As a consequence the slope of the drying fronts increase. Arrows indicate the final maximum signals S_{max} and thicknesses d of the coatings.

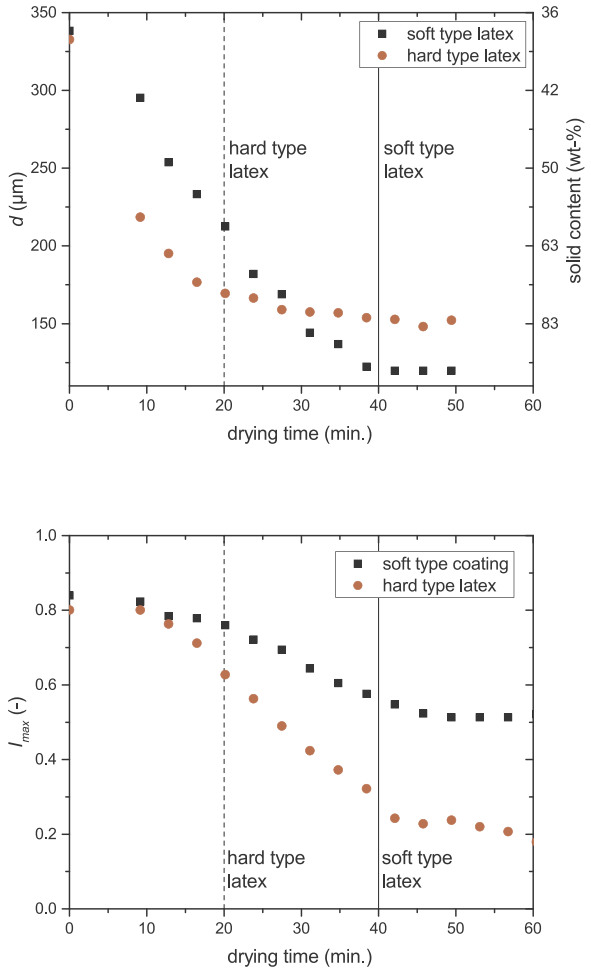

Fig. 2. Coating thicknesses of the hard and soft type latex (top) and maximum normalized signal intensity I_{max} (bottom) during drying. The front and bottom positions are arbitrarily taken at signal level $S = 0.5S_{max}$. The solid and dashed lines indicate the points at which the soft type and hard type latex dispersions, respectively, reach their closest packing of particles.

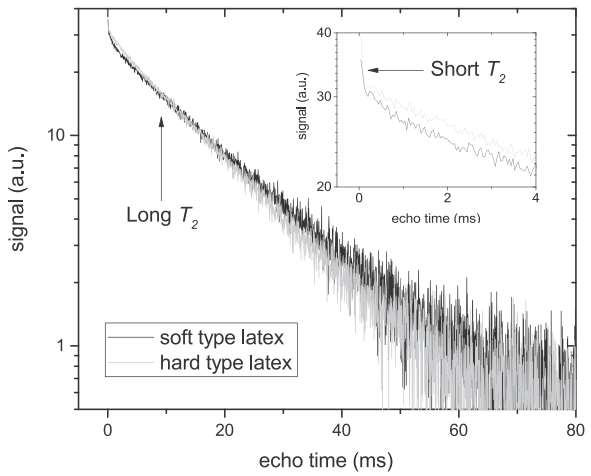

Fig. 3. Ostroff–Waugh signal decays of latex dispersions of the soft type (black) and hard type (gray) particles. The arrows indicate the short and long relaxations.

temperature, respectively, is discussed. This provides insight into the influence of the polymer particle packing morphology and deformation ability, governed by the particle T_g, on the mobility of water including

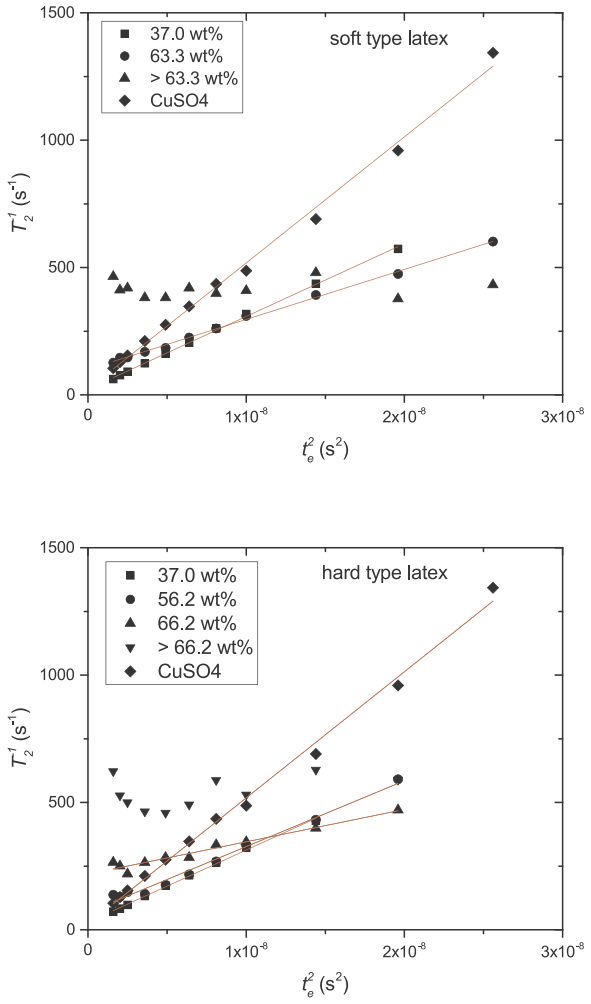

Fig. 4. Inverse $T_{2,long}$ as a function of t_e^2 for an aqueous 0.025 M $CuSO_4$ solution (diamonds), for non-dried latex (squares) and at different latex solid contents after drying at 80% *RH*. The solid lines are linear fits through the data points. The water diffusion coefficient D is determined from the slope of the curves and $T_{2,dip}$'s are determined from the inverse of the intercepts of the curves. Values for $T_{2,long}$ are taken at a position in the bulk, i.e. as close as possible to the bottom of the sample. Latex solid contents are determined from the coating thicknesses d.

free auto-diffusion, enclosed water evaporating through a polymer matrix and water that is physically bound to the polymer material. This will ultimately support research on the influence of water on the latex film formation process and how this can be used to develop latex dispersions that are fully plasticizable with water.

2. Materials and methods

2.1. Latex synthesis

The latices used for this study were supplied by DSM Coating Resins and were prepared via an emulsion copolymerization of *n*-butyl acrylate, methyl methacrylate, and methacrylic acid. The T_g of the latices could be varied by adjusting the ratio of butyl acrylate and methyl methacrylate. In Table 1, monomer compositions of two latices used are shown. The monomer amounts used in the synthetic procedure described below are those of the hard type latex.

A 2 L flask equipped with a thermometer, N_2 inlet and overhead stirrer was charged with water (858.7 g) and sodium lauryl sulphate (41.3 g; 30 wt.% solution in water) and heated to 85 °C, while stirring under nitrogen atmosphere. At 82 °C a solution of ammonium

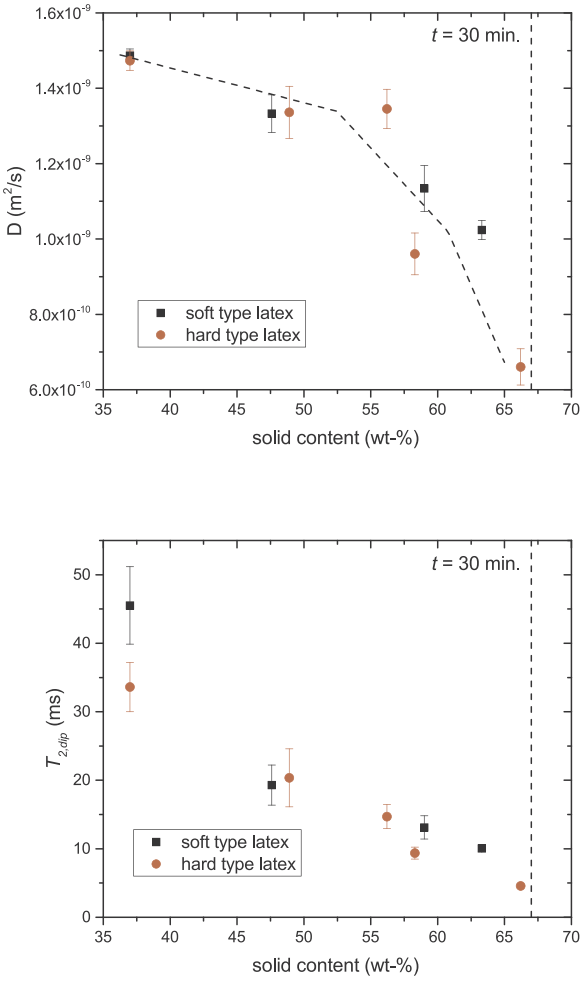

Fig. 5. Diffusion coefficients of the latex water (top) and $T_{2,dip}$ as a function of latex solid content. Data points are obtained by interrupting the drying process and performing echo time various experiments. The dashed line is drawn to guide the eye.

persulphate (2.7 g) in demineralized water (8.1 g) was added to the flask. Next, 5 wt.% of a mixture of methyl methacrylate (MMA; 376.5 g), *n*-butyl acrylate (*n*-BA; 135.5 g) and methacrylic acid (MAA; 27.0 g) was added to the flask and the temperature was allowed to increase to 85 °C. At 83–87 °C the remainder of the monomer mixture was added to the flask over 90 min. Subsequently, the funnel was rinsed with demineralized water (7.3 g), which was added to the flask. The flask was kept at 85 °C for 45 min, after which the temperature was decreased to 60 °C. During cooling, a solution of ammonia (7.9 g; 25 wt % in water) in demineralized water (16.0 g) was added. After addition of the ammonia solution, the mixture was allowed to cool down to room temperature. Finally, ProxelUltra10 (6.0 g) was added, followed by demineralized water (13.0 g). The resulting latex was filtered using a filter cloth to remove any coagulated material. The average particle diameter (Z_{av}) and polydispersity index (Đ) were determined by dynamic light scattering (Malvern Zetasizer Nano ZS) at 25 °C. The midpoint T_g of the dried latex materials was determined by DSC (TA Instruments Q2000) under a nitrogen atmosphere at a heating rate of 20 °C. The solid weight fractions were determined gravimetrically. Results of the analyses are listed in Table 2.

2.2. GARField ^{1}H NMR

GARField ^{1}H NMR imaging is a useful tool to describe drying of thin films and its design and principles have first been described by Glover et al. [14]. The magnetic field strength of the equipment used for this study was 1.5 T and the static gradient was 42.2 ± 0.2 T/m. From the signal decays of an Ostroff–Waugh [15] pulse sequence $(90°_x - \tau - [90°_y - \tau - \text{echo} - \tau]_n)$, T_2 relaxation times of both water and polymer are obtained. Unless stated otherwise, the echo time $t_e = 2\tau$ used for this study is 40 µs with an acquisition time t_{ac} of 35 µs, resulting in a spatial resolution of 14 µm. The long delay l_d was set at 1.7 s and the number of echoes n at 128. To reduce the signal-to-noise ratio, signal decays were obtained by averaging multiple measurements as follows: 20 decays of 64 averages, 10 decays of 256 averages, and 20 decays of 1024 averages. The results were normalized with a reference signal, obtained by a measurement on an aqueous 0.025 M $CuSO_4$ solution, with $t_e = 40$ µs, $t_{ac} = 35$ µs, $l_d = 0.3$ s, $n = 2048$ and 4096 averages.

To control the evaporation rate of the latex, the NMR set-up is equipped with a temperature and humidity controlled chamber in which the sample is placed directly onto the RF coil. This sample holder is a 140 µm thick cover glass covered with a microscope object glass having a circular hole with a 10 mm diameter. Herein, 37 µL of latex was placed using a 100 µL volumetric pipette, resulting in a wet coating of about 300 µm thickness. Initially, the sample holder is closed with a silicone stopper to perform a measurement without any drying. Subsequently, the cover is removed and sequential drying measurements are performed.

The Ostroff–Waugh signal decays of latex at a certain position in the film can be fitted with an exponential decay function,

$$S_n(x) = P_n(x)\sum_{k=1}^{N} A_k(x)\exp\left(\frac{-\mathrm{nt}_e}{T_{2,k}(x)}\right) + S_0 \quad (1)$$

where $S_n(x)$ is the total signal at time $t = nt_e$ [s], $T_{2,k}(x)$ [s] is the transversal relaxation time of the kth proton pool of the sample with amplitude $A_k(x)$, and S_0 is the signal noise level. $P_n(x)$ is a weighing factor necessary to correct for heterogeneities in the coil profile and echo modulations introduced by the Ostroff–Waugh sequence. $P_n(x)$ is obtained using an aqueous 0.025 M $CuSO_4$ solution. For details, we refer to [16]. With this, Eq. (1) can be re-written as

$$I_n(x) = \sum_{k=1}^{N}\frac{A_k(x)}{A_{\mathrm{ref}}(x)}\exp\left(\frac{-\mathrm{nt}_e}{T_{2,k}(x)}\right) = \sum_{k=1}^{N}\rho_k(x)\exp\left(\frac{-\mathrm{nt}_e}{T_{2,k}(x)}\right) \quad (2)$$

where $I_n(x)$ is the relative signal intensity and $\rho_k(x)$ the relative proton density of the kth proton pool with respect to water. $A_{ref}(x)$ is the signal amplitude obtained with a reference measurement of the 0.025 M $CuSO_4$ solution. The T_2 describes the relaxation processes of protons due to mobility [17–19] and diffusion [20,21].

The transversal relaxation time T_2 can be split in a dipole effect $T_{2,dip}$ [s], related to the local molecular mobility, and a diffusion part $T_{2,diff}$ [s] according to:

$$\frac{1}{T_2} = \frac{1}{T_{2,\mathrm{dip}}} + \frac{1}{T_{2,\mathrm{diff}}}. \quad (3)$$

The self-diffusion D [m^2/s] of water in latex is determined by acquisition of T_2 relaxation times at various t_e. The T_2 dependence on t_e is given by the following relation,

$$T_{2,\mathrm{diff}}^{-1} = \alpha\gamma^2G^2\mathrm{Dt}_e^2. \quad (4)$$

where α is a constant, which is determined experimentally, G [T/m] the field gradient, and γ [Hz/T] the gyromagnetic constant for proton atoms [22,23]. By determining the T_2 relaxations of an aqueous 0.025 M $CuSO_4$ reference solution at various t_e, Eq. (4) can be used to determine D for both latex dispersions taking $D = 2.3 \times 10^{-9}$ m^2/s for Ref. [24].

$T_{2,dip}$ can be approximated by

$$T_{2,\mathrm{dip}}^{-1} \sim \langle\omega^2\rangle\tau_c \quad (5)$$

where τ_c is the correlation time of the local molecular motions and $\langle\omega^2\rangle$

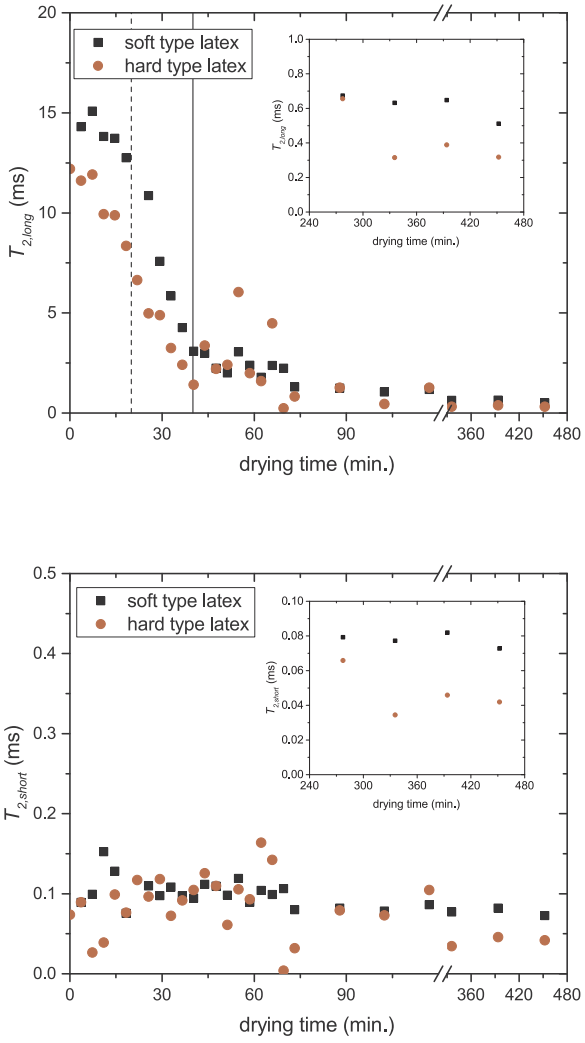

Fig. 6. The long (top) and short (bottom) T_2 relaxations of the hard and soft type latices during drying obtained by a double exponential fit of the Ostroff–Waugh signal decays using Eq. (1). The solid and dashed lines indicate the points at which the soft type and hard type latex dispersions reach their closest packing of particles, as shown in Fig. 2. T_2 values are taken at a position in the bulk, i.e. as close as possible to the bottom of the sample.

is the second moment associated with residual interactions [25,26,18]. If $\tau_c \ll t_e$ Eq. (5) holds. For more detailed discussion we refer to [16]. Therefore, using various echo times $T_{2,\mathrm{diff}}^{-1}$ and $T_{2,\mathrm{dip}}^{-1}$ can be determined.

2.3. Atomic force microscopy

After drying a latex film, the resulting coating was glued onto a metal disc and mounted on the sample stage of the AFM. AFM images were obtained under ambient conditions in tapping mode (NanoScope V multimode atomic force microscope, Bruker Nano Surfaces) using silicon cantilevers (TESP, Bruker Nano surfaces) with resonance frequencies of 300–400 kHz. Height scale and scan area are shown next to the AFM images.

3. Results

3.1. Proton distributions during drying

The drying of the latex dispersions can result in a heterogeneous distribution of water and polymer particles, which affects the drying rate and final coating structure. Therefore, it is important to study the proton distributions during drying. With GARField ^{1}H NMR proton distribution profiles during drying of latex can be obtained.

Drying experiments of the soft and hard type latex dispersions were done using GARField ^{1}H NMR as described in Section 2.2 (Exp. I). Fig. 1 shows the normalized proton distribution profiles of both the hard and soft type latex during drying at 80% *RH*. The drying shows the well-known two-step drying behavior.

First, a receding front is observed, indicating shrinkage of the layer due to evaporation of water and concomitant packing of the latex particles. It should be noted that the increased slope of the drying fronts is an effect of the averaging of drying profiles used to reduce noise. To compare water evaporation rates, Fig. 2 shows coating thicknesses d and maximum signal intensities I_{max} during drying. The sharper decrease of the hard latex thickness d_{hard} and signal intensity $I_{max,hard}$ refers to a higher drying rate for the hard type latex.

Second, d and I_{max} are leveling off to more constant values. The leveling of the soft latex thickness d_{soft} and signal intensity $I_{max,soft}$ appear to more or less coincide at approximately 40 min drying. The leveling of d_{hard} at approximately 20 min, however, does not coincide with the leveling of $I_{max,hard}$ at approximately 40 min, which suggests continuation of bulk water evaporation for this latex dispersion while

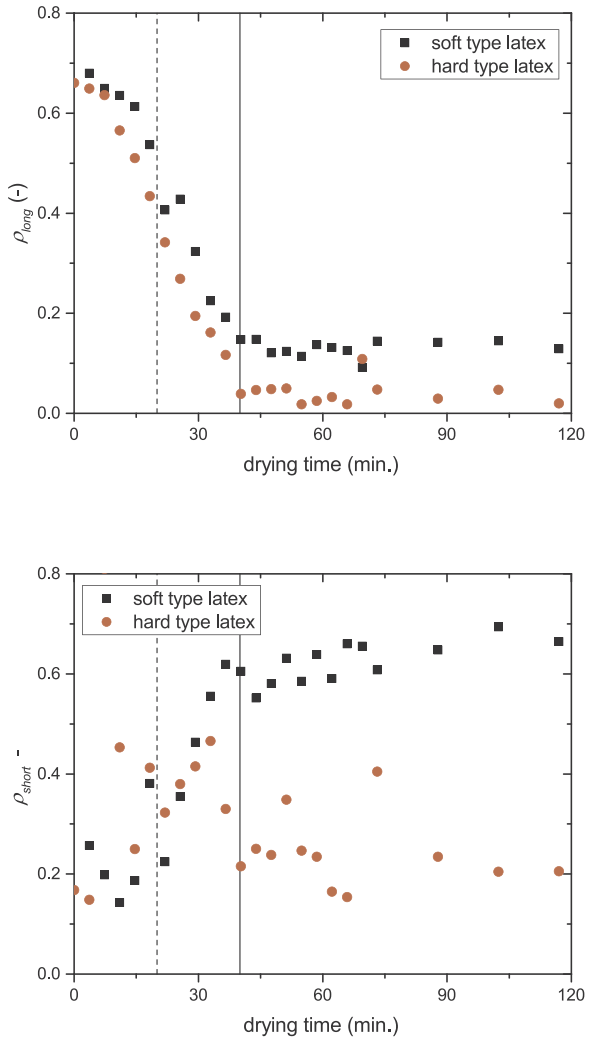

Fig. 7. Relative proton densities with respect to 0.025 M $CuSO_4$ of the long (ρ_{long}; top) and short (ρ_{short}; bottom) relaxations obtained by a double exponential fit of the Ostroff–Waugh signal decays using Eq. (2). The solid and dashed lines indicate the points at which the soft type and hard type latex dispersions reach their closest packing of particles, as shown in Fig. 2. Values for ρ are taken at a position in the bulk, i.e. as close as possible to the bottom of the sample.

latex particles are fixed in position and cannot deform and interdiffuse. This is in line with expectations for latex containing non-deformable and non-coalescing particles, which upon drying forms a brittle and porous network [1]. $I_{max,hard}$ after drying is also significantly lower than $I_{max,soft}$. This could be a result of the presence of empty pores and, therefore, less water in the hard coating, and different T_2 relaxation behavior may play a role. Additional relaxation analyses as discussed in Sections 3.2 and 3.3 are necessary for clarification.

3.2. Proton mobilities during drying

As a consequence of polymer particle compaction during drying, the water mobility in latex will be restricted. The auto-diffusion D and T_2 relaxation of water will decrease and interdiffusion of particles, and thus particle T_g, is expected to be of influence. Water protons and polymer protons of the latex dispersions have different T_2 relaxations. This T_2 is a measure of proton mobility, which can be determined by fitting an Ostroff–Waugh signal decay with Eq. (1) using $k = 2$, thus assuming two proton pools with different mobilities. Using an Ostroff–Waugh pulse sequence, measurements were done on both latex

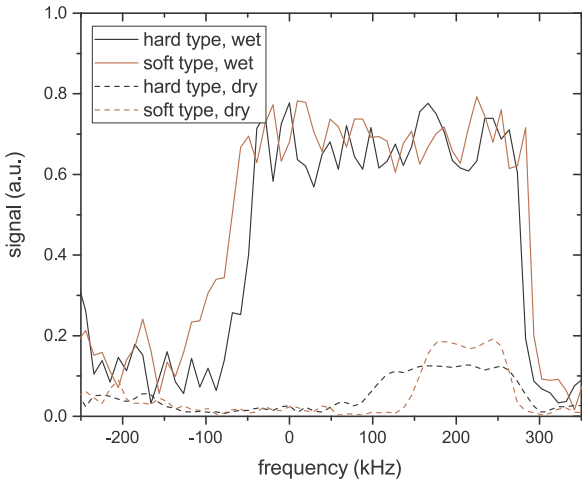

Fig. 8. Proton distribution profiles of layers of hard type (black solid) and soft type (red solid) latex and the resulting hard type (black dashed) and soft type (red dashed) coatings after 24 h drying at 80% *RH* and subsequently 48 h at with $CaCl_2$. t_e was set at 100 µs and t_{ac} at 90 µs to increase the spatial resolution for an accurate determination of the front positions. (For interpretation of the references to color in this figure legend, the reader is referred to the web version of this article.)

dispersions (Exp. II). The sample cups were closed to prevent evaporation of water. In Fig. 3 the resulting Ostroff–Waugh decays are shown. A short $T_{2,short}$ and long $T_{2,long}$ relaxation time can be identified for both latices, each corresponding to proton atoms with a different mobility.

As was mentioned in Section 2.2, T_2 relaxations can consist of a diffusion part ($T_{2,diff}$) and a dipolar part ($T_{2,dip}$). The contributions of $T_{2,diff}$ and $T_{2,dip}$ can be investigated by determining D of water during the drying process on the basis of t_e variation measurements. For this, drying experiments (Exp. III) were done similar to those discussed in Section 3.1, but the drying process was stopped by closing the sample cup. Subsequently, t_e variation measurements were done. For each data point, a separate experiment was done and stopped at a different drying time. Fig. 4 shows examples of the results of these experiments at different solid contents, derived from the coating thicknesses d, during the drying process for both the soft and hard type latex using the $T_{2,long}$ relaxations. The $T_{2,short}$ relaxations do not vary with t_e and are therefore not used to determine D of water. From the slope of the curves in Fig. 4, D is determined using Eq. (4) and $T_{2,dip}$ is determined with the inverse of the intercept of the curves. In Fig. 5 D and $T_{2,dip}$ during drying of both latex dispersions are shown.

Before drying, both values for D_{soft} and D_{hard} are similar and in the same order of that of free water. Therefore, it is concluded that the long T_2 component represents the latex water phase. As expected D decreases during drying. At approximately 30 min drying, this is at latex solid contents above 67%, D could not be measured anymore.

$T_{2,dip}$ of both latex dispersions also decreases. This can be explained with the increasing surface-to-volume ratio of latex particles and water during drying, which increases the interaction of water with the latex particle surface.

Although after approximately 30 min drying there is no measurable D of water anymore, significant amounts of water are still present in between the closer packed particles. Continued drying of the latex dispersions can still reduce T_2 relaxations and, therefore, water mobilities. Fig. 6 shows short and long T_2 relaxation times obtained from experiment I at a position in the bulk, i.e. as close as possible to the bottom of the sample holder. As expected, the long T_2 relaxation time decreases during drying due to limitations in proton mobility by an increased interaction of water molecules with the latex particles. Initially, $T_{2,long}$ is higher for the soft type latex, which suggests more

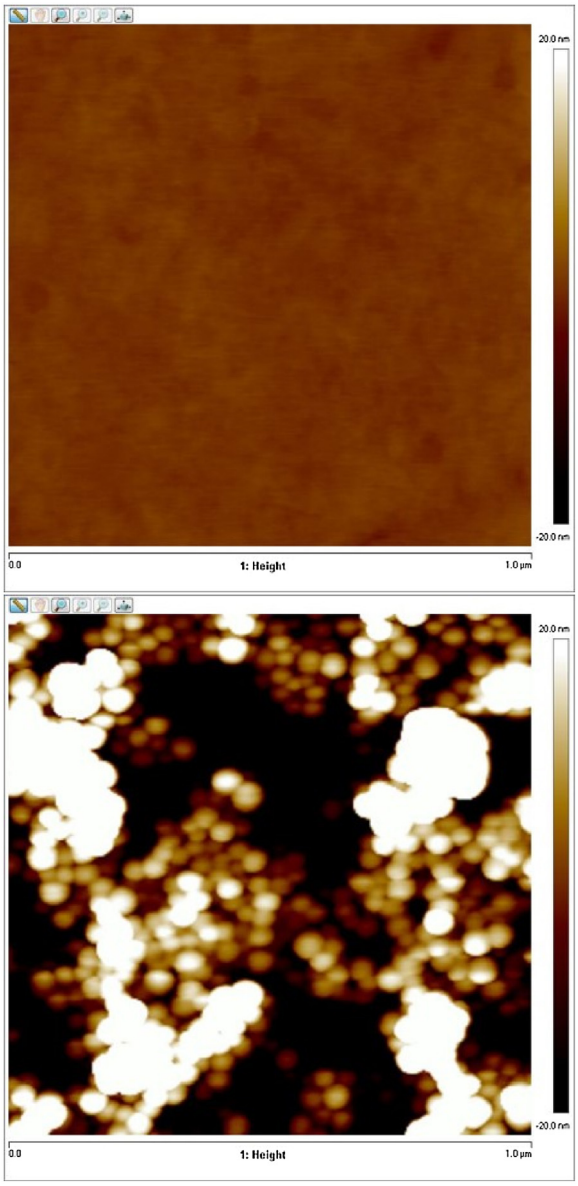

Fig. 9. Tapping mode AFM images of the surfaces of a soft type (top) and hard type (bottom) coating.

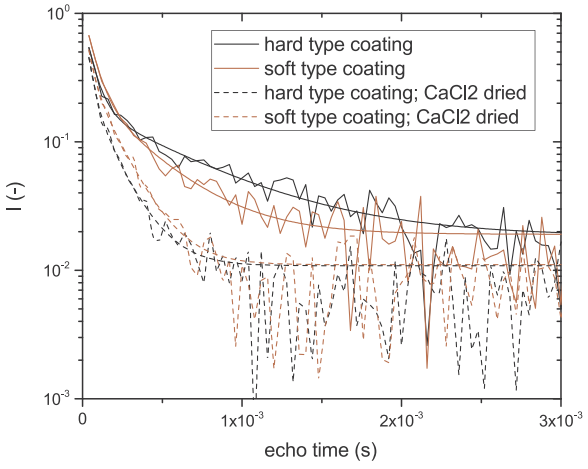

Fig. 10. Ostroff–Waugh decays of the soft and hard type coatings saturated at 80% *RH* and after additional drying for 48 h with anhydrous $CaCl_2$.

Table 3
T_2's of the hard and soft type coatings after drying at 80% *RH* for 24 h and after additional drying with anhydrous $CaCl_2$ for 48 h.

Coating	Drying condition	$T_{2,short}$ (ms)	$T_{2,long}$ (ms)
Hard type	80% *RH*	0.06	0.69
Hard type	+ $CaCl_2$	0.04	0.17
Soft type	80% *RH*	0.07	0.39
Soft type	+ $CaCl_2$	0.04	0.17

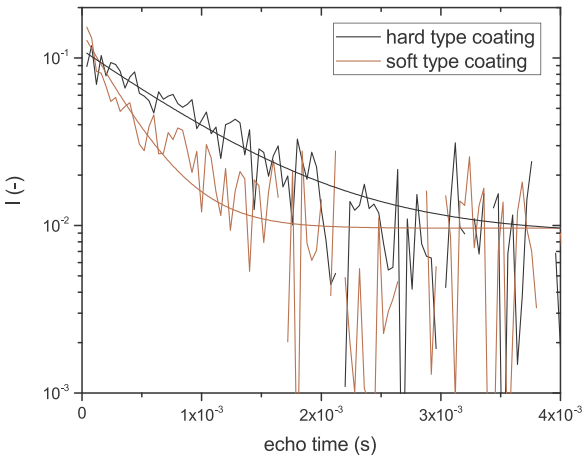

Fig. 11. Ostroff–Waugh decays of the soft and hard type coatings obtained by subtraction of the decays of the 80% *RH* saturated coatings with the decays of the coatings after 48 h additional drying with $CaCl_2$.

mobile water-polymer interaction affecting $T_{2,dip}$. During the first 20 min drying, $T_{2,long}$ of the soft type latex appears to remain more constant and decreases rapidly for the hard type latex. After 20 min drying, $T_{2,long}$ of the hard type latex decreases at a similar rate, but decreases more rapidly for the soft type latex. After approximately 40 min drying, the $T_{2,long}$'s of both latex dispersions level off to an equilibrium value. The final $T_{2,long}$ of the soft type latex is higher than that of the hard type latex. To explain this phenomenon, more information on the state of the residual water is necessary.

The $T_{2,short}$'s for both latex dispersions remain constant at approximately 0.1 ms during drying. Evidently, both latex dispersions have proton pools with similar mobilities that do not change as a result of the evaporation of bulk water. These relaxations are therefore attributed to protons embedded in the latex particles, which are not affected by the evaporation of water. The relative proton density changes during drying are shown in Fig. 7. The proton densities of the $T_{2,long}$ (ρ_{long}) decrease during drying for both latex dispersions. Again, ρ_{long} for both latex dispersions levels off at approximately 40 min, which coincides with the results for the soft type latex shown in Fig. 2 but not for the hard type latex. The proton densities for $T_{2,short}$ (ρ_{short}), however, show an increase for the soft type latex, but appears constant for the hard type latex, which suggests further concentrating of the latex polymer phase for the soft type latex.

3.3. Coating structure and proton mobility

In a coating, water can be present either in pores or pockets in a liquid state, or in a state of physically bound to the polymer matrix. Both states influence the coating physical and mechanical properties in their own way, and as such it is necessary to know how water is distributed in a coating. As was mentioned in Section 2.2, Eq. (2) can be used to provide insight into the proton densities of the latices. For a dry coating, proton densities of both polymer and residual water can be determined. Using proton balance equations, the absence of signal is an indication for air-filled voids, pores, or cracks. Here an assumption is

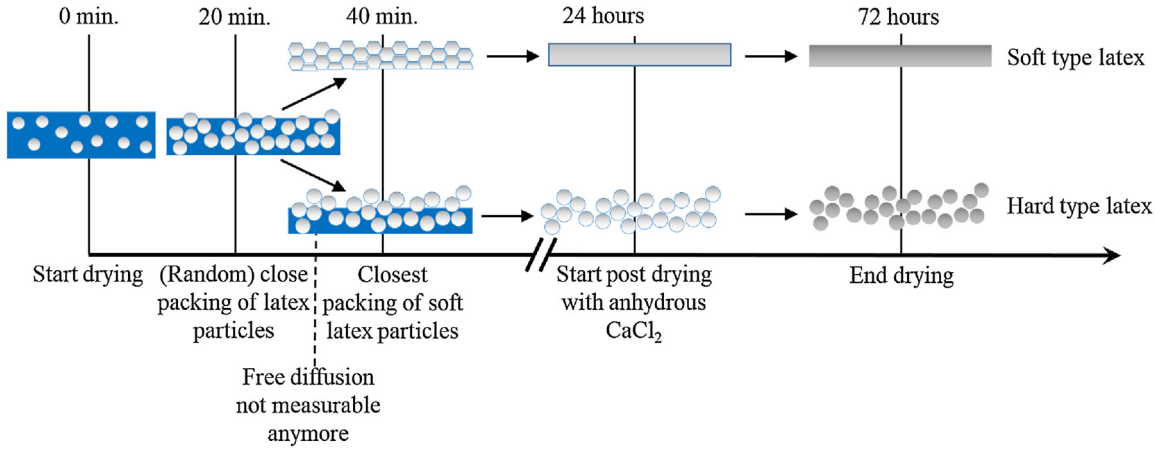

Fig. 12. Visual representation of the drying process of the hard and soft type latex. At the start of the process, polymer particles are moving freely through the water phase. After approximately 20 min particles for both latex dispersions are closely packed due to the evaporation of water. At this point, the drying behavior differentiates. The soft latex particles deform upon further evaporation of water resulting in their closest packing morphology, whereas the hard latex particles remain in a fixed position. After 24 h drying, the soft type latex has formed a coherent coating due to particle interdiffusion. The hard type latex has formed a brittle coating due to the absence of particle interdiffusion. Additional drying with $CaCl_2$ for another 48 h results in harder coatings due to the removal of water, which acts as a plasticizer for the polymers.

made that between the excitation pulse and the first echo, no decay of a rigid group of protons occurs. Since, $T_{2,long}$ is successfully used to determine D for water, its presence after drying of latex can be an indication of water-filled voids or physically bound water.

A first order approximation of the coating porosity can be made by studying the thickness of a wet latex layer and the resulting coating after drying. Thicknesses of wet latex layers were measured by determination of the width of the first echo profile obtained with an Ostroff–Waugh pulse sequence with $t_e = 100\,\mu s$, $t_{ac} = 90\,\mu s$, $n = 256$, and 256 averages. The increase of t_e and t_ac with respect to the procedure described in Section 2.2 was necessary to improve the spatial resolution and thus the accuracy of the measurements. After 24 h drying at 80% *RH* an additional drying step was introduced by placing the sample cups in a closed vessel containing anhydrous $CaCl_2$ for 48 h to ensure full evaporation of water. The thicknesses of the dry coatings were assessed using the same procedure that was used to determine the thicknesses of the wet latex layers. Fig. 8 shows proton distribution profiles of layers of the hard and soft type latex, both for the initial, wet situation and the resulting coatings after drying are shown.

Taking both front positions and sample bottom positions at $S = 0.5S_{max}$ the thickness of the wet layers and dried coating can be determined. The void fraction ϕ_0 of the coating can be calculated,

$$\phi_0 = \frac{V_0}{V_{\text{coat}}} = 1 - \frac{H_{\text{pol}}}{H_{\text{coat}}}, \tag{6}$$

with V_0 and V_{coat} the volume of the void space and the total coating volume, respectively. V_0 is either taken up by water or air present in the coating. H_{pol} is the theoretical thickness of the coating when film formation is complete and no air or water is present in the coating, and H_{coat} is the actual thickness of the coating. This can be re-written as

$$\phi_0 = 1 - \phi_{\text{pol}} \frac{H_{\text{wet}}}{H_{\text{coat}}}, \tag{7}$$

where H_{wet} is the thickness of the wet latex layer and ϕ_{pol} is the polymer volume fraction in the latex. On the basis of this, void volume fractions are estimated at 0.37 and 0.08 for the hard type coating ($\phi_{\text{void}}^{\text{hard}}$) and soft type coating ($\phi_{\text{void}}^{\text{soft}}$), respectively. AFM was used to analyze the surfaces of both hard and soft type coatings and to reflect on the void volume fraction results. In Fig. 9, images show a featureless soft type coating surface, whereas the hard type coating shows packed un-coalesced particles.

Fig. 10 shows Ostroff–Waugh decays of the coatings after 24 h drying of the latex at 80% *RH* and after the additional drying step with anhydrous $CaCl_2$, of which the first echo profiles are shown in Fig. 8. Both coatings at 80% *RH* show a clear double exponential decay, which could indicate residual water present in the coating. After the additional drying step the decays shorten, but the fit of the curves still show the presence of two proton pools. In Table 3, T_2 values obtained from fits of the Ostroff–Waugh decays are listed. $T_{2,long}$ and $T_{2,short}$ of both coatings decrease after 48 h drying with $CaCl_2$.

It is possible that the T_2 relaxations in the coatings are mixed polymer and water signals. Calculating "residual curves" by subtracting the post-dried decays from the 80% *RH* decays could provide decays for the residual water in the 80% *RH* coatings. These results in Fig. 11 can be fit with single exponential decay functions, indicating a single pool of protons for both coatings, which can be attributed to water. The hard type coating appears be more affected by the presence of water at 80% *RH*.

3.4. Discussion

In the previous sections different stages of the drying process have been discussed in which the mobility of water changes from free to pore water and water that is physically bound to the polymer matrix. In this section a comprehensive overview is given. In Fig. 12, a visual representation is given of a plausible drying mechanism of the hard and soft type latex.

Initially, latex particles and water are able to move freely. Water proton mobility and water diffusion decrease due to an increased interaction with the polymer particle surface, concomitantly decreasing $T_{2,dip}$ as is shown in Fig. 5. After approximately 20 and 40 min drying at 80% *RH* for the hard and soft type latex, respectively, the thicknesses of the coatings do not decrease significantly anymore, as shown in Fig. 2. At this point, however, the hard type latex still contains considerable amounts of bulk water, which can evaporate freely through the voids between the non-deformable and non-coalescing particles. This is confirmed by the results in Figs. 2, 6 and 7, which show further decrease of $I_{max,hard}$, $T_{2,long}$, and ρ_{long} between 20 and 40 min for the hard type latex occurring with the proceeding release of water from the coating.

After 24 h drying at 80% *RH*, Ostroff–Waugh decays still show two proton pools, which can be explained either by the presence of free water in inter-particle voids, or by the presence of water bound to the polymer matrix plasticizing domains with different hardness in the

coating. Fig. 8 indeed shows the presence of void space, in particular for the hard type coating, which could hold water. Further drying under anhydrous $CaCl_2$ for 48 h shows a definite change in signal in Fig. 10. The Ostroff–Waugh decays still show two proton pools. Two things can be extracted from these results.

First, $T_{2,short}$ and $T_{2,long}$ found during the entire drying process do not result from the polymer and water protons, respectively, but both are a mix of the polymer and water signals. In the first stage of the drying process, $T_{2,long}$ is dominated by D of water for both latex dispersions, and therefore $T_{2,diff}$ as described by Eq. (3). After closer packing of the polymer particles, however, the dipolar component $T_{2,dip}$ dominates the relaxation behavior.

Second, since no water is expected to be left in the coatings after the additional drying step with $CaCl_2$, the presence of two proton pools can be explained by domains in the coatings having different degrees of hardness. The softer domain for the hard type coating appears to be more sensitive to the presence of water, as is shown by the more obvious change in relaxation after post-drying with $CaCl_2$. Due to the more hydrophilic nature of the hard type coating because of the presence of more MMA and less *n*-BA with respect to the soft type coating, the plasticizing effect of the polymer is more obvious. On the basis of these results it can be concluded that the T_2 relaxations in the coatings are mixed polymer and water signals. Earlier work by Reuvers showed that crystalline and amorphous domains in polyamides were found [27]. Similarities can be drawn here, where harder and softer domains could be present in the hard and soft type coatings even after post-drying under $CaCl_2$.

4. Conclusion

The possibility of a latex to form a coherent coating is determined by a number of factors. The polymer particle glass transition temperature T_g is an important factor as it determines the flexibility of polymer chains and, therefore, influences the ability of particles to deform, which enables polymer interdiffusion. The drying behavior of two acrylic latex types was studied with GARField ^{1}H NMR, with focus on the mobility of water: a hard type latex with a dry polymer T_g above room temperature (RT) and a soft type latex with a polymer T_g below RT. Relaxometry measurements were performed 23 °C and 80% relative humidity (*RH*).

The mobile state of water during drying of the latex dispersions is elucidated. Two pools of protons were found, that appear to be a mix of water and polymer protons. During a first stage of the drying process, the water is diffusing freely and it is shown that the diffusion coefficient D is dependent on the solid content of the latex. After this first stage, a significant amount of water is still present in both dispersions and the proton mobilities become dependent on the latex particle packing morphology and deformation ability, governed by the particle T_g. For the soft type latex, it was found that proton mobility is decreasing more rapidly due to deformation of particles and interdiffusion of polymers. After 24 h drying, water present in the hard and soft coating is plasticizing two polymer phases with a different degree of hardness. The hard coating is plasticized stronger due to the more hydrophilic nature of the polymer chains.

The drying process of latex dispersions is influenced by additives present in the dispersions. The ionic strength of both latex dispersions should therefore be comparable for both latex dispersions. For future work, studying the influence of sodium dodecyl sulphate (SDS) and other ionic content on the drying behavior of these latex dispersions is recommended.

Acknowledgements

This work is part of the research programme True Solvent Free (TSoF) – Towards the next generation of waterborne coatings with project number 13157, which is (partly) financed by the Netherlands Organisation for Scientific Research (NWO). The authors would like to thank Qi Chen (DSM Coating Resins) for providing the AFM images and Joseph Keddie (University of Surrey) for his valuable feedback.

References

[1] J.L. Keddie, A.F. Routh, Fundamentals of Latex Film Formation, 1st ed., Springer, Dordrecht, The Netherlands, 2010.
[2] A.F. Routh, Drying of thin colloidal films, Rep. Prog. Phys. Phys. Soc. (Great Britain) 76 (April (4)) (2013) 046603.
[3] A.F. Routh, W.B. Russel, Deformation mechanisms during latex film formation: experimental evidence, Ind. Eng. Chem. Res. 40 (October (20)) (2001) 4302–4308.
[4] E.M. Boczar, B.C. Dionne, Z. Fu, A.B. Kirk, P.M. Lesko, A.D. Koller, Spectroscopic studies of polymer interdiffusion during film formation, Macromolecules 26 (21) (1993) 5772–5781.
[5] J. Feng, H. Pham, V. Stoeva, M.A. Winnik, Polymer Diffusion in Latex Films at Ambient Temperature, (October 1997), pp. 1129–1139.
[6] J.C. Haley, Y. Liu, M.A. Winnik, D. Demmer, T. Haslett, W. Lau, Tracking polymer diffusion in a wet latex film with fluorescence resonance energy transfer, Rev. Sci. Instrum. 78 (August (8)) (2007) 084101.
[7] A.C. Hellgren, M. Wallin, P.K. Weissenborn, P.J. McDonald, P.M. Glover, J.L. Keddie, New techniques for determining the extent of crosslinking in coatings, Prog. Org. Coat. 43 (November (1–3)) (2001) 85–98.
[8] J. Mallégol, G. Bennett, P.J. Mcdonald, J.L. Keddie, O. Dupont, Skin development during the film formation of waterborne acrylic pressure-sensitive adhesives containing tackifying resin, J. Adhes. 82 (April (3)) (2006) 217–238.
[9] J. Mallégol, J.P. Gorce, O. Dupont, C. Jeynes, P.J. McDonald, J.L. Keddie, Origins and effects of a surfactant excess near the surface of waterborne acrylic pressure-sensitive adhesives, Langmuir 18 (May (11)) (2002) 4478–4487.
[10] F.T. Carter, R.M. Kowalczyk, I. Millichamp, M. Chainey, J.L. Keddie, Correlating particle deformation with water concentration profiles during latex film formation: reasons that softer latex films take longer to dry, Langmuir 30 (32) (2014) 9672–9681.
[11] S.J.F. Erich, L.G.J. van der Ven, H.P. Huinink, L. Pel, K. Kopinga, Curing processes in solvent-borne alkyd coatings with different drier combinations, J. Phys. Chem. B 110 (April (15)) (2006) 8166–8170.
[12] A.M. König, T.G. Weerakkody, J.L. Keddie, D. Johannsmann, Heterogeneous drying of colloidal polymer films: dependence on added salt, Langmuir 24 (July (14)) (2008) 7580–7589.
[13] P. Ekanayake, P.J. McDonald, J.L. Keddie, An experimental test of the scaling prediction for the spatial distribution of water during the drying of colloidal films, Eur. Phys. J. Spec. Top. 166 (February (1)) (2009) 21–27.
[14] P.M. Glover, P.S. Aptaker, J.R. Bowler, E. Ciampi, P.J. McDonald, A novel high-gradient permanent magnet for the profiling of planar films and coatings, J. Magn. Reson. (San Diego, CA: 1997) 139 (July (1)) (1999) 90–97.
[15] E.D. Ostroff, J.S. Waugh, Multiple spin echos and spin locking in solids, Phys. Rev. Lett. 16 (24) (1966) 1097–1099.
[16] V. Baukh, H.P. Huinink, O.C.G. Adan, S.J.F. Erich, L.G.J. van der Ven, Water–polymer interaction during water uptake, Macromolecules 44 (12) (2011) 4863–4871.
[17] R. Kimmich, N. Fatkullin, Polymer Chain Dynamics and NMR vol. 1, (2004).
[18] P. Sotta, C. Fülber, D.E. Demco, B. Blümich, H.W. Spiess, Effect of residual dipolar interactions on the NMR relaxation in cross-linked elastomers, Macromolecules 29 (19) (1996) 6222–6230.
[19] V.M. Chernov, G.S. Krasnopol'skii, Nuclear magnetic relaxation, correlation time spectrum, and molecular dynamics in a linear polymer, J. Exp. Theor. Phys. 107 (2) (2008) 302–312.
[20] H.Y. Carr, E.M. Purcell, Effects of diffusion on free precession in nuclear magnetic resonance experiments, Phys. Rev. 94 (3) (1954) 630–638.
[21] M.D. Hürlimann, Diffusion and relaxation effects in general stray field NMR experiments, J. Magn. Reson. 148 (2) (2001) 367–378.
[22] R.M.E. Valckenborg, H.P. Huinink, J.J.v.d. Sande, K. Kopinga, Random-walk simulations of NMR dephasing effects due to uniform magnetic-field gradients in a pore, Phys. Rev. E Stat. Phys., Plasmas, Fluids, Relat. Interdiscip. Top. 65 (2) (2002) 1–8.
[23] J. Petković, H.P. Huinink, L. Pel, K. Kopinga, Diffusion in porous building materials with high internal magnetic field gradients, J. Magn. Reson. 167 (1) (2004) 97–106.
[24] K. Krynicki, C.D. Green, D.W. Sawyer, Pressure and temperature dependence of self-diffusion in water, Faraday Discuss. Chem. Soc. 66 (1978) 199.
[25] J.H. Van Vleck, Dipolar broadening, Phys. Rev. 74 (9) (1948) 1168–1183.
[26] W. Gründer, H. Schmiedel, D. Freude, Eine neue Methode zur Messung von Korrelationszeiten mit Hilfe von NMR-lmpulsverfahren, Ann. Phys. 7 (27) (1971) 409–416.
[27] N. Reuvers, H. Huinink, O. Adan, Water plasticizers only a small part of the amorphous phase in nylon-6, Macromol. Rapid Commun. 34 (11) (2013) 949–953.